Early thymectomy leads to premature immunologic ageing: An 18-year follow-up

To the Editor:

Early thymectomy is routinely performed in infants undergoing cardiac surgery as the thymus lies anterior to the heart in the mediastinum obstructing the surgeon's access. Early cardiac surgery has become more common in the last decades and in Sweden, with close to 10 million inhabitants, approximately 250 infants are thymectomized (Tx) annually. The population of Tx individuals is thus increasing both in numbers and in age. The ultimate effect of early thymectomy is still obscure although immunologic alterations have been described. Lymphocyte subsets are affected with a T-cell lymphopenia, characterized by a decrease in naive T cells with a concomitant increase in the memory T-cell population.[1-3] The effects of thymectomy on the regulatory T (Treg)-cell population differ between studies. One study showed that although the absolute Treg-cell number was lower, the Treg-cell proportion was increased, albeit with a decrease in naive Treg cells.[4] T-cell receptor excision circles (TRECs) have consistently been found to decrease after thymectomy although to varying degrees.[2,3] Studies published to date have not shown any alteration in overall disease risk, but generally the groups are small and often heterogeneous, with a lack of information on the amount of thymic tissue that was removed and with a short follow-up time. Here, we present results from a prospective study of the immunologic impact of early thymectomy (age, <6 months, >90% thymic removal, n = 11) with blood samples collected preoperatively, at 18 months, and 18 years later.

Group characteristics and clinical data are presented in Tables E1 and E2 (see this article's Online Repository at www.jacionline.org). Multivariate factor analysis (orthogonal projection to latent structures discriminant analysis) reveals a clear distinction between Tx individuals and healthy controls (Fig 1, *A* and *B*). A decrease in T-cell number was apparent and consistent over time in the Tx group (see Table E3 in this article's Online Repository at www.jacionline.org; Fig 1, *C-G*). Of interest is that the Tx group had a decreased number of lymphocytes, particularly T cells (Table E3; Fig 1, *H*), even preoperatively. At the 18-year follow-up, the number of naive helper T cells ($CD45RA^+$) was lower in the Tx group than in controls (0.15 vs 0.49 $\times$ 10^9/L; $P < .0001$) whereas the memory helper T cells ($CD45RO^+$) were unaffected (0.34 vs 0.30 $\times$ 10^9/L; $P = .48$), thereby showing a proportional increase in relation to the already low $CD4^+$ T-cell number (Fig 1, *I* and *J*). In cytotoxic T cells, the same was true: absolute $CD8^+CD45RA^+$ naive T-cell number was lower in cases (0.11 vs 0.35 $\times$ 10^9/L; $P = .0002$) but the $CD8^+CD45RO^+$ memory T-cell number was unaffected (0.11 vs 0.13 $\times$ 10^9/L; $P = .27$) (Fig 1, *K* and *L*). The cell surface marker CD31 has been defined as a marker of recent thymic emigrants.[5] Tx individuals showed a lower proportion of $CD31^+$ helper T cells (55% vs 81%; $P = .034$), but with a wide range (25% to 89%), whereas the results for the control group were higher and not as wide-ranging (76% to 90%) (Fig 1, *M*). There was a linear correlation between naive $CD4^+$ and $CD8^+$ cells, indicating that Tx individuals were similarly affected in both subsets (Fig 1, *N*). Also, the Tx group (black circles) is clearly distinct from the control group (open circles) with a lower number of both $CD4^+$ and $CD8^+$ naive T cells. The total number of Treg cells was lower in the Tx group than in controls (0.035 vs 0.053 $\times$ 10^9/L; $P = .0417$) (Fig 2, *A*). The proportions, however, were unaffected (6.5% vs

METHODS

Study design and participants

Patients with cutaneous granulomas and with diverse PIDs were selected from the USIDNET registry. Additional cases (cases 1 and 11) were recruited from the CIS immune deficiency Listserv. Hospitals participating in the study submitted archival patient material to the Children's Hospital of Philadelphia, where specimens were anonymized and then sent to the Rubella Global Specialized Laboratory (Centers for Disease Control and Prevention [CDC], Atlanta, Ga) to be tested blindly.

Tissue samples

Slides were cut from archived formalin-fixed, paraffin-embedded (FFPE) tissue samples, which were routinely collected for diagnosis according to standards of practice. Tissue sections of skin biopsies were taken from 19 patients with granulomatous diseases: 14 patients with PID and 5 patients without PID (pyoderma gangrenosum, cutaneous Crohn disease, nonspecific granulomatous dermatitis, histiocytosis, and granulomatous inflammation of the face). FFPE skin tissues from nongranuloma cases were used as negative control material. Fresh-frozen skin tissue was received and tested for RV by the CDC Laboratory as a part of reference/surveillance responsibilities. RV detection analysis for this case was conducted for the purpose of public health response and was not considered to be human research. Archived FFPE specimens from all patients were tested anonymously, with a nondisclosure agreement, which was determined to be ethically acceptable by the Internal Review Board at the CDC.

Immunofluorescence staining of FFPE tissue sections

For immunofluorescence studies, 3- to 4-μm tissue sections were deparaffinized in Histoclear II (National Diagnostics, Atlanta, Ga) and rehydrated using a series of ethanol washes. Epitope retrieval was performed by heating deparaffinized tissue sections in citrate buffer (10 mM sodium citrate, pH 6.0, 0.05% Tween 20) for 20 minutes at 98°C and cooling down in the same buffer for 20 minutes. After this and each subsequent immunostaining step, the sections were washed 3 times, 5 minutes each, in 1× PBS. Tissues were permeabilized with 0.05% Tween-20 in 1× PBS for 45 minutes at room temperature. Nonspecific binding of fluorescent dyes to tissues was reduced by incubation with Image-iT FX signal enhancer (Thermo Fisher Scientific, Waltham, Mass) for 30 minutes at room temperature. Nonspecific antibody-binding sites were blocked with BlockAid solution (Thermo Fisher Scientific) for 1 hour at room temperature. Tissue sections were then incubated with either mouse monoclonal anti-RV capsid antibody (Abcam, Cambridge, United Kingdom) or a mixture of capsid antibody with each of rabbit cell-type–specific mAb or polyclonal antibody (diluted with BlockAid to the working concentration) at 4°C overnight. Types of antibodies, their suppliers, and working dilutions are listed in Table E5. Incubation with the secondary antibody, goat anti-mouse IgG Alexa Flour-555, and anti-rabbit IgG Alexa Flour-488 (Molecular Probes, Waltham, Mass) diluted 1:1000 in BlockAid was carried out for 1 hour at room temperature followed by counterstaining with 4′-6-diamidino-2-phenylindole, dihydrochloride (Invitrogen, Carlsbad, Calif). Autofluorescence was blocked by incubating sections in 0.3% Sudan black solution in 70% ethanol for 10 minutes at room temperature followed by a brief rinse in 70% ethanol and 3 PBS washes (Fig E2). Cells were mounted with fluorescence- mounting medium (Dako, Carpinteria, Calif). Images were acquired with a Zeiss fluorescent microscope using AxioVision software (Carl Zeiss, Thornwood, NY).

Specificity of RV capsid immunostaining in patient tissues was confirmed by probing sequential tissue sections with the different RV-specific antibodies, either mouse anticapsid RV mAb (produced by CDC core facility), rabbit polyclonal antibody against purified RV virions (produced by CDC core facility), or RV capsid antibody (manufactured by Abcam). The RV antibodies were preabsorbed with either human proteins (mixture of A459 and HUVEC cell lysates) (Fig E3) or purified RV virions (Fig E4; results for only RV polyclonal antibody are shown). Sections from an FFPE block containing a mixture of uninfected and RV-infected A549 human lung carcinoma cells (ATCC#CCL-185) served as a positive control in each immunofluorescence assay.

In addition, *negative controls* were run in parallel in each assay and consisted of sequential tissue sections of case patients incubated with mAb to measles virus nucleoprotein or mengovirus RNA polymerase. Negative tissue control was also performed in each assay and consisted of a noncase FFPE skin section incubated with the RV antibody. Each test was repeated at least once. Interpretation of IF assay results included determination of the location of the RV-positive signal in a tissue, the type of cells infected, and the intensity of staining.

Virus isolation

Skin biopsy tissue from case 1 was cut into small pieces and then homogenized in high glucose Dulbecco's modified Eagle medium (Invitrogen) containing 5% FBS (Atlanta Biologicals, Lawrenceville, Ga) supplemented with 50 μg/mL gentamicin (Invitrogen) with Bead Beater (Sigma, Valencia, Calif) tissue homogenizer using 1.5-mm zirconium beads (Sigma Aldrich, St Louis, Mo). The tissue homogenate was then inoculated onto monolayers of WI-38 human fetal fibroblasts (Coriell Cell Repository, Camden, NJ) and Vero cells (ATCC #CCL-81). Both media and cells were passaged 3 times weekly. Real-time RT-PCR for RV RNA and infectivity titration on Vero cells were performed to monitor the infected cultures for the presence of RV in the culture media. After each passage, the cells were seeded into chamber slides, fixed with methanol, and then subjected to indirect immunofluorescence for RV structural proteins and *in situ* hybridization for RV genomic RNA as described elsewhere.[E1,E2]

Molecular analyses

RNA was isolated from a frozen skin sample using an RNeasy Fibrous Tissue Mini Kit (Qiagen, Valencia, Calif) according to the manufacturer's instructions. Primers and conditions for real-time RT-PCR for measles, mumps, and RVs, genotyping RT-PCR, a detailed strategy for a whole-genome sequencing, and phylogenetic analyses have been described.[E1,E3-E6]

REFERENCES

E1. Perelygina L, Zheng Q, Metcalfe M, Icenogle J. Persistent infection of human fetal endothelial cells with rubella virus. PLoS One 2013;8:e73014.
E2. Perelygina L, Adebayo A, Metcalfe M, Icenogle J. Differences in establishment of persistence of vaccine and wild type rubella viruses in fetal endothelial cells. PLoS One 2015;10:e0133267.
E3. Abernathy E, Chen MH, Bera J, Shrivastava S, Kirkness E, Zheng Q, et al. Analysis of whole genome sequences of 16 strains of rubella virus from the United States, 1961–2009. Virol J 2013;10:32.
E4. Namuwulya P, Abernathy E, Bukenya H, Bwogi J, Tushabe P, Birungi M, et al. Phylogenetic analysis of rubella viruses identified in Uganda, 2003-2012. J Med Virol 2014;86:2107-213.
E5. Hummel KB, Lowe L, Bellini WJ, Rota PA. Development of quantitative gene-specific real-time RT-PCR assays for the detection of measles virus in clinical specimens. J Virol Methods 2006;132:166-73.
E6. Rota JS, Rosen JB, Doll MK, McNall RJ, McGrew M, Williams N, et al. Comparison of the sensitivity of laboratory diagnostic methods from a well-characterized outbreak of mumps in New York city in 2009. Clin Vaccine Immunol 2013;20:391-6.

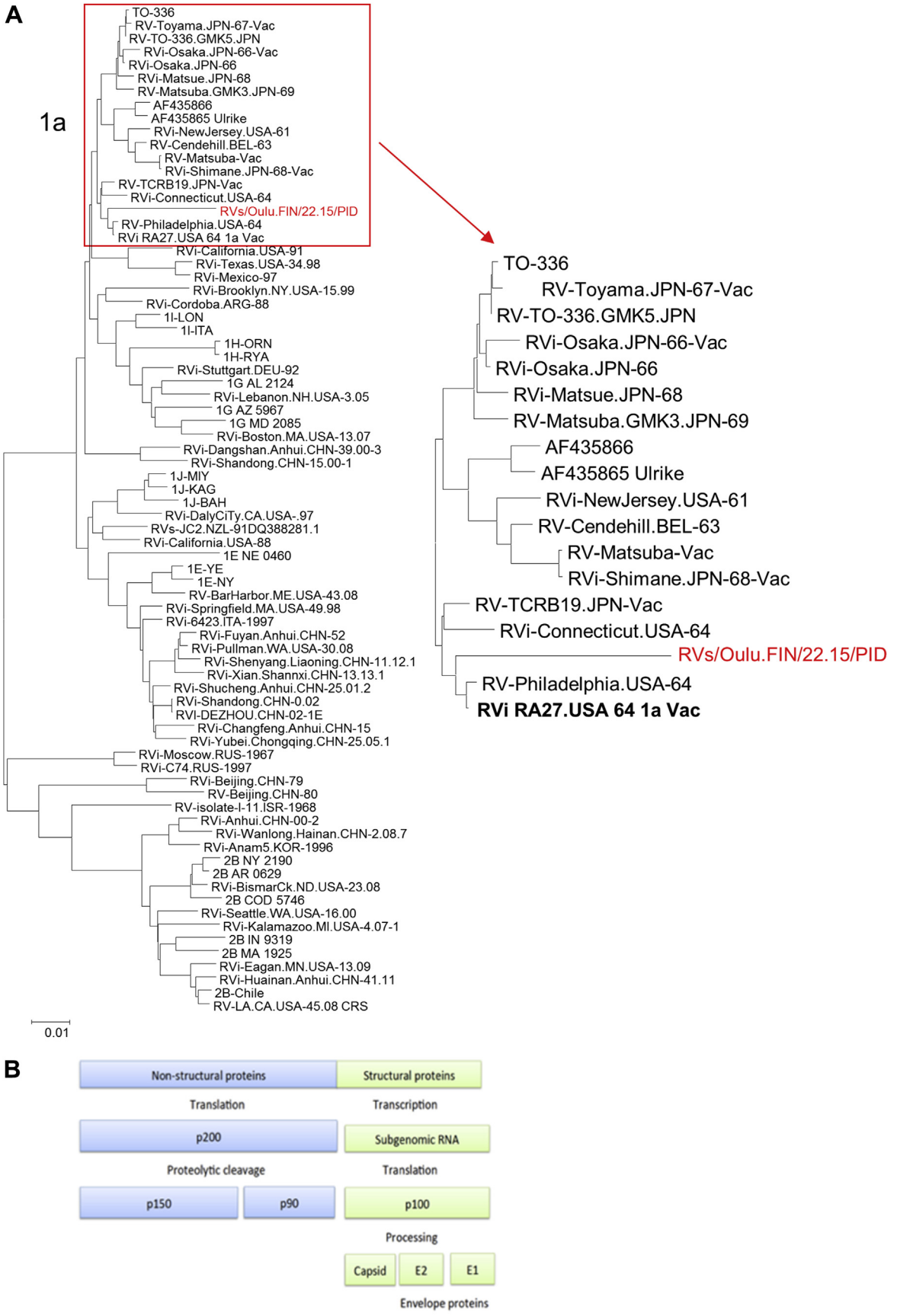
A
1a
TO-336
RV-Toyama.JPN-67-Vac
RV-TO-336.GMK5.JPN
RVi-Osaka.JPN-66-Vac
RVi-Osaka.JPN-66
RVi-Matsue.JPN-68
RV-Matsuba.GMK3.JPN-69
AF435866
AF435865 Ulrike
RVi-NewJersey.USA-61
RV-Cendehill.BEL-63
RV-Matsuba-Vac
RVi-Shimane.JPN-68-Vac
RV-TCRB19.JPN-Vac
RVi-Connecticut.USA-64
RVs/Oulu.FIN/22.15/PID
RV-Philadelphia.USA-64
RVi RA27.USA 64 1a Vac
RVi-California.USA-91
RVi-Texas.USA-34.98
RVi-Mexico-97
RVi-Brooklyn.NY.USA-15.99
RVi-Cordoba.ARG-88
1I-LON
1I-ITA
1H-ORN
1H-RYA
RVi-Stuttgart.DEU-92
1G AL 2124
RVi-Lebanon.NH.USA-3.05
1G AZ 5967
1G MD 2085
RVi-Boston.MA.USA-13.07
RVi-Dangshan.Anhui.CHN-39.00-3
RVi-Shandong.CHN-15.00-1
1J-MIY
1J-KAG
1J-BAH
RVi-DalyCiTy.CA.USA-.97
RVs-JC2.NZL-91DQ388281.1
RVi-California.USA-88
1E NE 0460
1E-YE
1E-NY
RV-BarHarbor.ME.USA-43.08
RVi-Springfield.MA.USA-49.98
RVi-6423.ITA-1997
RVi-Fuyan.Anhui.CHN-52
RVi-Pullman.WA.USA-30.08
RVi-Shenyang.Liaoning.CHN-11.12.1
RVi-Xian.Shannxi.CHN-13.13.1
RVi-Shucheng.Anhui.CHN-25.01.2
RVi-Shandong.CHN-0.02
RVI-DEZHOU.CHN-02-1E
RVi-Changfeng.Anhui.CHN-15
RVi-Yubei.Chongqing.CHN-25.05.1
RVi-Moscow.RUS-1967
RVi-C74.RUS-1997
RVi-Beijing.CHN-79
RV-Beijing.CHN-80
RV-isolate-I-11.ISR-1968
RVi-Anhui.CHN-00-2
RVi-Wanlong.Hainan.CHN-2.08.7
RVi-Anam5.KOR-1996
2B NY 2190
2B AR 0629
RVi-BismarCk.ND.USA-23.08
2B COD 5746
RVi-Seattle.WA.USA-16.00
RVi-Kalamazoo.MI.USA-4.07-1
2B IN 9319
2B MA 1925
RVi-Eagan.MN.USA-13.09
RVi-Huainan.Anhui.CHN-41.11
2B-Chile
RV-LA.CA.USA-45.08 CRS
0.01
TO-336
RV-Toyama.JPN-67-Vac
RV-TO-336.GMK5.JPN
RVi-Osaka.JPN-66-Vac
RVi-Osaka.JPN-66
RVi-Matsue.JPN-68
RV-Matsuba.GMK3.JPN-69
AF435866
AF435865 Ulrike
RVi-NewJersey.USA-61
RV-Cendehill.BEL-63
RV-Matsuba-Vac
RVi-Shimane.JPN-68-Vac
RV-TCRB19.JPN-Vac
RVi-Connecticut.USA-64
RVs/Oulu.FIN/22.15/PID
RV-Philadelphia.USA-64
RVi RA27.USA 64 1a Vac
B
Non-structural proteins
Structural proteins
Translation
Transcription
p200
Subgenomic RNA
Proteolytic cleavage
Translation
p150
p90
p100
Processing
Capsid
E2
E1
Envelope proteins

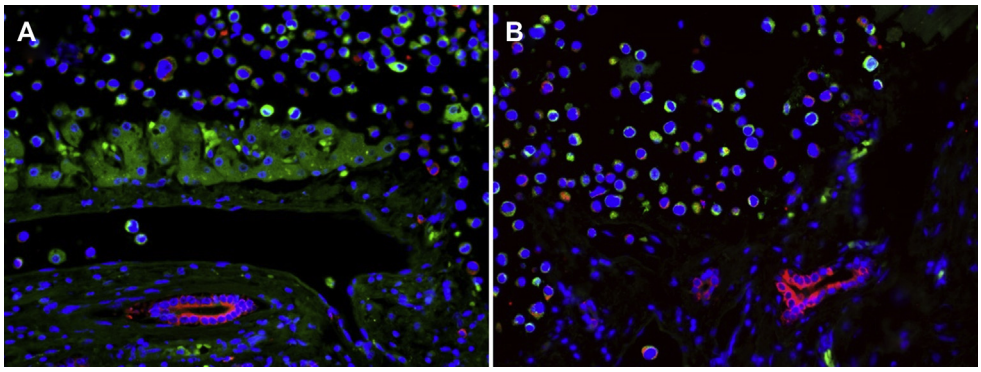

FIG E2. RV-positive control slides containing a mixture of 4 human tissues and RV-infected A459 cell double immunostained with capsid mAb and pan-keratin polyclonal antibody and counterstained with DAPI. The slides were either untreated **(A)** or treated **(B)** with 0.3% Sudan *black* solution before mounting. Note the reduction in autofluorescence after Sudan *black* treatment (Fig E2, *B*). *DAPI*, 4′-6-Diamidino-2-phenylindole, dihydrochloride.

FIG E1. The genetic relationships between the full rubella genome sequences were inferred using the Neighbor-Joining method. **A,** The tree is composed of 76 rubella viruses, including sequences of RA27/3 vaccine (bold) and RVs/Oulu.FIN/22.15/PID *(red)*. Sequences were obtained from the GenBank or from Dr Min-hsin Chen. The genetic distances were computed using the maximum composite likelihood method. The scale bar indicates the number of base substitutions per site. The recovered virus sequence is clearly related to the vaccine strain RVI RA27.USA 64 1a vac. **B,** RV genome organization. The rubella genome is a single-strand RNA virus of positive polarity. The 2 open reading frames are denoted by *blue* and *green* boxes. Individual proteins after processing of the 2 polyproteins are shown below.

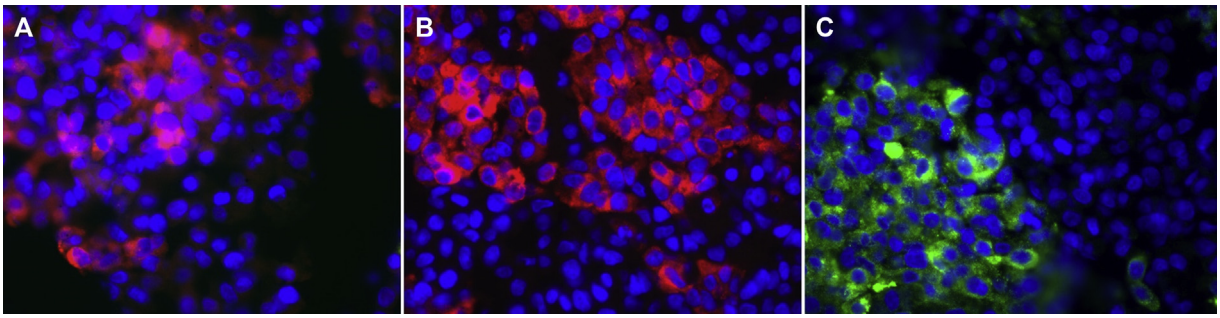

FIG E3. Histological immunofluorescent staining of positive control slides with either rabbit RV polyclonal antibody (CDC) **(A)**, mouse capsid mAb (Abcam) **(B)**, or mouse capsid mAb (CDC) **(C)**, which were preabsorbed with human proteins. Anti-rabbit IgG Alexa Flour-555 (Fig E3, *A*), anti-mouse IgG Alexa Flour-555 (Fig E3, *B*), or Alexa Flour-488 (Fig E3, *C*) served as secondary antibody; nuclei were counterstained with DAPI. *DAPI*, 4′-6-Diamidino-2-phenylindole, dihydrochloride.

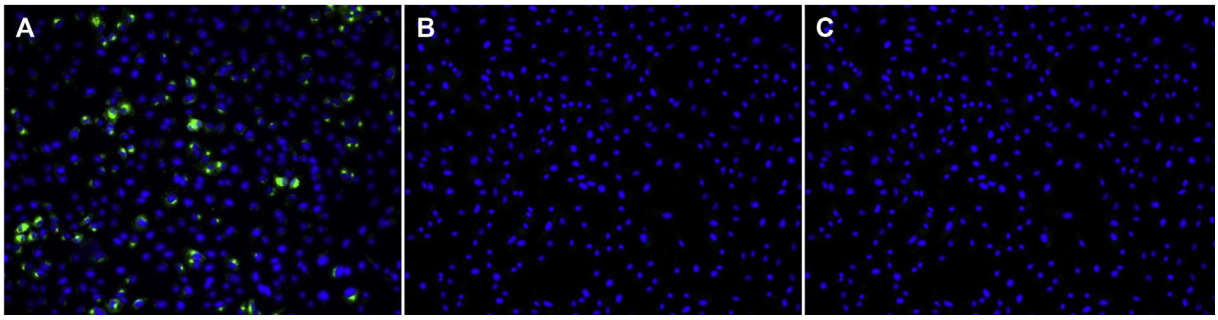

FIG E4. Specificity of rabbit RV polyclonal antibody (CDC). Immunofluorescent staining of Vero cells infected with rubella virus (**A** and **B**) with either RV polyclonal or RV polyclonal preabsorbed with purified RV virions. **C,** Mock-infected Vero cells. Note the lack of specific staining with the antibody preabsorbed with the specific antigen.

TABLE E1. Characterization of RV-positive cells in skin tissues of patients with PID by double immunostaining with cell-type–specific antibodies

Antigen	Cell type	Costaining with capsid
CD1a	Langerhans cells	N
CD3	T cells	N
CD11c	Myeloid dendritic cells	N
CD20	B cells	N
vWF	Endothelial cells	N
CD14	Monocytes/macrophages	Y
CD68	Macrophages, dendritic cells	Y
CD163	M2-activated macrophages	Y
CD206	M2-activated macrophages	Y
iNOS	M1-activated macrophages	N
Pan-cytokeratin	Keratinocytes	Y

TABLE E2. Vaccine-specific amino acids (aa) in RV proteins

	p150 aa			p90 aa	Capsid aa		E1 aa
Genomes	**3**	**541**	**1209**	**93**	**18**	**48**	**210**
RA27/3	R	V	S	V	T	T	H
Other RV	K	A	P or L	I	A	S	Y
RVs/Oulu.FIN/22.15/PID	R	V	S	V	**A**	T	**Y**

Boldface with underline indicates reversions to wild-type aa in the patient's virus.

TABLE E3. Amino acid substitutions in RVs/Oulu.Fin/22.15/PID

No.	Protein	Amino acid				Notes
		Position	RA27/3	RVs/Oulu.Fin/22.15/PID	Other 75 viruses	
1	**p150**	203	V	A*	V	
2		251	D	H	D, E	
3		427	G	D	D, G	
4		464	R	C	R, H	
5		488	A	T	A	
6		507	R	P	R, G	Q-domain (aa 497-717), includes hypervariable region (HVR, aa 697-803)
7		551	A	V	A, V, T	
8		700	A	V	A, T	
9		718	A	T	A, S, V	
10		728	P	L	P, S, L	
11		730	P	S	P, S	
12		740	S	P	S, P, L, M, A, T	
13		746	P	L	P	
14		751	A	V	A, V	
15		757	P	T	P	
16		797	P	S	P, S, T, A	
17		799	S	L	P, S, T, A	
18		821	L	I	L	ADP-ribose binding, domain (aa 814-966)
19		883	H	Y	H	
20		996	P	L	P	
21		1014	R	C	H, P, R	Protease domain (aa 1000-1300)
22		1017	S	P	S, P, L	
23		1025	D	N	D, E	
24		1117	V	A	M, V, I	
25	**p90**	67	R	C	R	Helicase domain (aa 19-308)
26		115	I	V	I	
27		582	N	S	N	RdRp catalytic domain (aa 569-680)
28		694	H	Y	H	
29		703	P	S	P	
30	**C**	18	T	A	A	Vaccine-specific aa
31		118	P	S	P	
32		119	R	H	R	
33		125	P	S	P	
34		141	L	P	L, P	
35		163	E	V	E	
36		166	V	T	V	
37		228	A	V	A, T	
38		237	T	M	T	
39		262	T	I	T, I	
40		267	T	I	T	
41		295	V	L	V, A	
42	**E2**	51	H	Y	H, Y	
43		109	A	V	A	
44		111	S	P	S, A, T, F	
45		112	T	M	T, I	
46		116	T	A	T, A, P	
47		134	G	D	G	
48		136	L	S	L	
49		165	Y	F	Y	
50		211	V	A	V	
51		218	T	I	T, I, A	
52		223	S	L	S	
53		230	A	T	A	
54		235	L	F	L	
55		266	A	V	A	
56	**E1**	34	A	V	A	
57		57	V	A	V, L, I	
58		70	P	S	P	
59		84	F	L	F, L	
60		95	Y	H	Y	

(Continued)

TABLE E3. (*Continued*)

No.	Protein	Amino acid				Notes
		Position	RA27/3	RVs/Oulu.Fin/22.15/PID	Other 75 viruses	
61		210	H	Y	Y	Vaccine-specific aa
62		280	I	T	I	
63		329	V	I	V	
64		415	P	S	P	
65		429	T	I	T	
66		437	Q	E	Q	
67		440	A	V	A, V	
68		444	A	T	A	
69		445	A	S	A	

*Boldface with underline denotes amino acids, which are unique for RVs/Oulu.Fin/22.15/PID.

TABLE E4. Changes in the antigenic structure of RV antigens of RVs/Oulu.FIN/22.15/PID relative to RA27/3 vaccine

Epitope	Epitope sequence in vaccine virus	Substitutions in patients' virus
Neutralizing B-cell epitopes		
$E1_{214-233}$*	QQSRWGLGSPNCHGPDWASP	None
$E1_{245-251}$	LVGATPE	None
$E1_{260-266}$	ADDPLLR	None
$E1_{274-285}$	VWVTPV**I**GSQAR	$I_{280} \rightarrow T$
$CD8^+$ T-cell epitopes		
C_{9-22}	MEDLQKALE**T**QSRA	$T_{18} \rightarrow A$
C_{11-29}	DLQKALE**T**QSRALRAELAA	$T_{18} \rightarrow A$
$C_{264-272}$	RIE**T**RSARH	$T_{267} \rightarrow I$

*Immunodominant epitope.

TABLE E5. Primary antibodies used for the immunofluorescence assay

Antigen	Type	Vendor	Catalog no.	Dilution
CD1a [EP3622]	Rb mAb	Abcam	ab108309	1:200
CD3 [SP7]	Rb mAb	Abcam	ab16669	1:200
CD11c [EP1347Y]	Rb mAb	Abcam	ab52632	1:200
CD20 [EP459Y]	Rb mAb	Abcam	ab78237	1:200
vWF	Rb Pab	Sigma	F3520	1:500
CD14 [EPR3653]	Rb mAb	Abcam	ab1899915	1:100
CD68	Rb Pab	Abcam	ab125047	1:100
CD163 [EPR14643-36]	Rb mAb	Abcam	Ab189915	1:500
CD206	Rb Pab	Abcam	ab64693	1:200
iNOS	Rb Pab	Novus	NBP1-33780	1:200
Pan-cytokeratin	Rb Pab	Abcam	ab9377	1:500
Rubella capsid	Ms mAb	Abcam	ab34749	1:500
Rubella capsid	Ms mAb	CDC	NA	1:500
Rubella virions	Rb Pab	CDC	NA	1:2000
Measles NP [83KKII]	Ms mAb	Millipore	MAB8906-KC	1:500
Mengo 3DPol [3B7]	Ms mAb	Santa Cruz	sc-65633	1:500

NA, Not available/applicable; *Pab*, polyclonal antibody.